1

History and Introduction of QDs and QDLEDs

Semiconductor nanocrystals (NCs) are the most widely studied of the nanoscale semiconductors. In early 1981, Alexei Ekimov and Alexander Efros, working at the S.I. Vavilov State Optical Institute and A.F. Ioffe Institute, Russia, discovered nanocrystalline, semiconducting quantum dots (QDs) in a glass matrix and conducted pioneering studies of their electronic and optical properties. Simultaneously, in 1985, Louis Brus at Bell Laboratories in Murray Hill, NJ, discovered colloidal semiconductor NCs (QDs), for which he shared the 2008 Kavli Prize in Nanotechnology. Over the years, QDs have been established as a new type of semiconductor nanocrystalline material whose size is smaller than or close to the excitonic Bohr radius of its bulk material. Common semiconductor materials include Si, Ge, compounds of group II–VI (e.g. CdSe), and compounds of group III–V (e.g. indium phosphide [InP]). When the size of these bulk semiconductor materials is larger than their exciton Bohr radii, electrons and holes are able to move freely and independently in the bulk materials. However, when the size of QDs is smaller than their own exciton Bohr radius, after being excited by light, an electron in the valence band will leap to the conduction band, leaving a hole in the valence band, and the electron and hole form an exciton due to Coulomb effect, which is confined in a space smaller than the exciton Bohr radius, and the electron and hole will be quantized, which is called the "quantum size effect" of nanomaterials. This quantum size effect allows QDs to have discrete energy levels, thus giving them unique physicochemical properties [1]. Colloidal semiconductor NCs have size-dependent particle properties, while their surface ligands make them solution-processable, which gives them a "particle-solution" duality.

Figure 1.1a shows the energy level diagrams of molecular, QD, and bulk semiconductor materials. The molecular orbital energy level diagram is composed of the highest occupied molecular orbital (HOMO) and the lowest unoccupied molecular orbital (LUMO), while the energy level diagram of QDs consists of some discrete energy levels, and the bulk semiconductor material consists of conduction and valence bands. Figure 1.1b illustrates the spatial extent of the confined domains of electrons and holes and the respective energy as a function of the density of electronic states for bulk semiconductor materials, two-dimensional

Colloidal Quantum Dot Light Emitting Diodes: Materials and Devices, First Edition. Hong Meng.

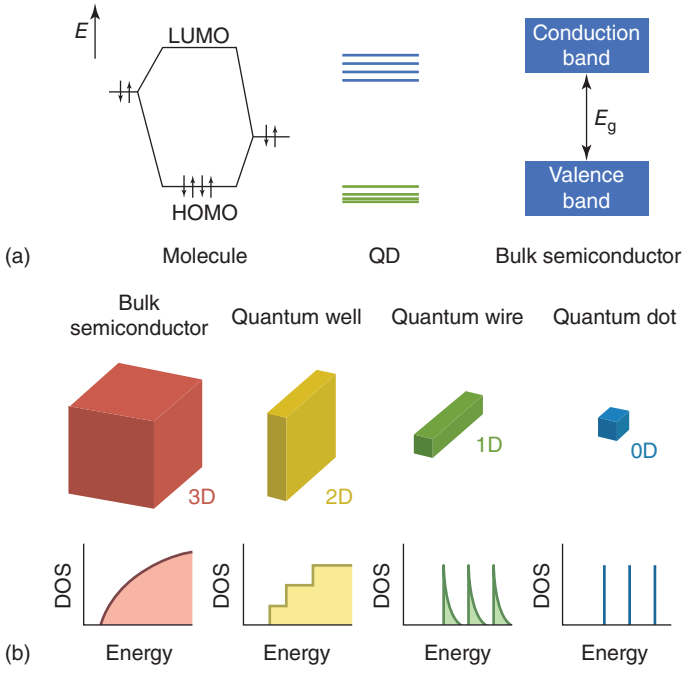

Figure 1.1 (a) Schematic diagram of energy levels of molecular, quantum dot, and bulk semiconductor materials; (b) spatial extent of the confined domain of electrons and holes and the respective energy as a function of the density of electronic states for bulk semiconductor materials, two-dimensional quantum sheets, one-dimensional quantum wires, and zero-dimensional quantum dots depending on the material size.

quantum sheets, one-dimensional quantum wires, and zero-dimensional QDs, depending on the size of the material. For a bulk semiconductor material, the dimensions in all three dimensions are larger than its own Bohr exciton radius, and electrons and holes are free to move independently in all three dimensions; while for a two-dimensional quantum sheet, the dimensions in two dimensions are larger than its own Bohr exciton radius, and electrons and holes are free to move independently in two dimensions; and for a one-dimensional quantum wire, the dimensions in one dimension are larger than its own Bohr exciton radius, while for a one-dimensional quantum wire, the dimensions in one dimension are larger than its own Bohr exciton radius, and electrons and holes are free to move independently in two dimensions. For a one-dimensional quantum wire, whose dimension in one dimension is larger than its own exciton radius, electrons and holes are free to move independently in one dimension; and for a zero-dimensional QD, whose dimension in all three dimensions is smaller than its own exciton radius, electrons and holes are restricted from moving freely and independently in all dimensions. In general, QD is a collective term for a two-dimensional quantum sheet, a one-dimensional quantum wire, and a zero-dimensional QD.

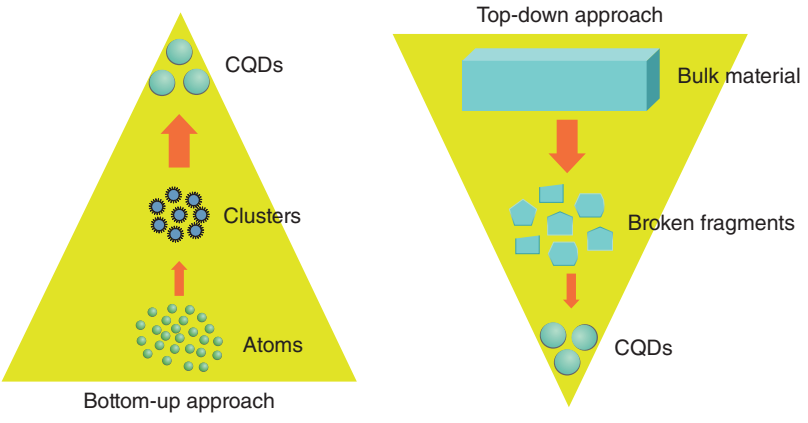

Figure 1.2 Preparation pathways for quantum dots: the "top-down" method and the "bottom-up" method.

1.1 Preparation Route of Quantum Dots

There are two completely different ways to prepare QDs, namely the "top-down method" and the "bottom-up method", as shown in Figure 1.2. The top-down method is to prepare QDs by reducing the dimensionality and size of the bulk semiconductor material; the bottom-up method is to combine atoms or molecules into QDs by chemical synthesis. The former approach is limited by the ultra-fine processing technology, which cannot produce QDs below 10 nm at present, and the morphological regulation of QDs is also limited to some extent. The latter is mainly achieved through colloidal chemical synthesis, which can produce colloidal QDs of different sizes and shapes.

1.2 Light-Emitting Characteristics of Quantum Dots

1.2.1 Particle Size and Emission Color

QDs are semiconductor particles having a few nanometers in size, their optical and electronic properties are quite different from those of larger particles as a result of quantum mechanics. When the QDs are illuminated by UV light, an electron in the QD can be excited from the transition of an electron valence band to the conductance band. The excited electron can drop back into the valence band releasing its energy as light. The color of that light depends on the energy difference between the conductance band and the valence band. The QD absorption and emission features correspond to transitions between discrete quantum mechanically allowed energy levels in the box, which are reminiscent of atomic spectra.

1.2.2 Quantum Dot Optical Property

The QDs are defined as the semiconductor NCs with the quantum confinement. Thus, the semiconductor nanoparticles with dimensions QDs have the following features:

1.2.2.1 Quantum Surface Effect

The surface effect refers to the fact that as the particle size of QDs decreases, most of the atoms are located on the surface of QDs, and the specific surface area of quantum dots increases with decreasing particle size. Due to the large specific surface area of QDs (nanoparticles), the increase in the number of atoms in the surface phase leads to the lack of coordination, unsaturated bonds, and suspension bonds of surface atoms. This makes these surface atoms highly reactive, extremely unstable, and easily bonded with other atoms. This surface effect will cause the large surface energy and high activity of nanoparticles. The activity of surface atoms not only causes changes in the surface atomic transport and structural type of nanoparticles but also causes changes in the surface electron spin conformation and electronic energy spectrum. This feature offers a route to manipulate QD interactions with their environment. QDs can be tethered to proteins, antibodies, or other biologic species and used as optically addressable bio-labels. On the other hand, passivation of QD surface can improve the QD stability and increase the photoluminescent quantum efficiency. Surface defects lead to trapped electrons or holes, which in turn affect the luminescent properties of QDs and cause nonlinear optical effects. Metallic materials show various characteristic colors through light reflection. Due to the surface effect and size effect, the light reflection coefficient of nanoparticles decreases significantly, usually less than 1%, so nanoparticles are generally black in color, and the smaller the particle size, the darker the color, i.e. the stronger the light absorption ability of nanoparticles, showing a broadband strong absorption spectrum. Surface effect or ligand modification offers an additional tool for manipulating energy levels and electronic and optical properties.

1.2.2.2 Quantum Size Effect

Quantum size effect refers to the phenomenon that the electron energy levels near the Fermi energy level change from quasi-continuous to discrete energy levels, that is, when the particle size drops to a certain value, the energy level splits or energy gap widens, in other words, the energy spectrum becomes discrete, and as a result, the bandgap becomes size-dependent. When the change in energy level is greater than the change in thermal, optical, and electromagnetic energy, it leads to the magnetic, optical, acoustic, thermal, electrical and superconducting properties of nanoparticles being significantly different from those of conventional materials. This feature of QDs is that the energy gap changes with the increase in the grain size, the larger the grain size, the smaller the energy gap, and *vice versa*, the larger the energy gap. That is, the smaller the QD, the shorter the wavelength of light (blueshift), and the larger the QD, the longer the wavelength of light (redshift). According to the size effect of QDs, we can use the method of changing the size of the grain to regulate

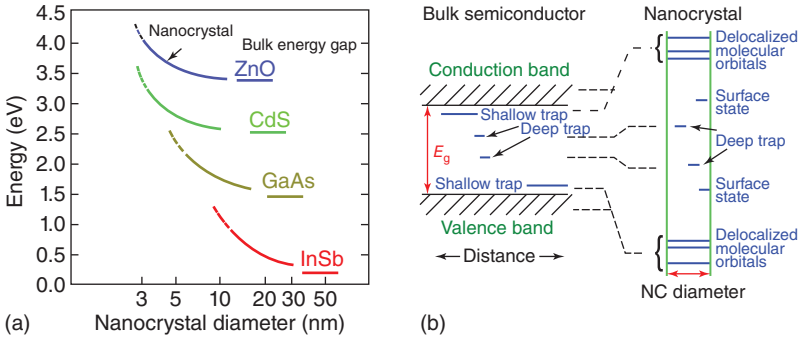

Figure 1.3 Theoretical ideas from the early 1980s. (a) Calculated size-dependent shift of the lowest exciton levels in strong confinement (b) Spatial electronic state correlation diagram for bulk semiconductors and NCs. The bulk valence and conduction bands, together with shallow trap states, evolve into the NC molecular orbitals. Deeply localized defect states in the bulk have essentially the same energy as those in the NC. New localized surface states exist in the NC. Source: Efros and Brus [2]/American Chemical society.

the tuning of the light spectrum of the material and no longer need to change the chemical composition of QDs.

1.2.2.3 Quantum Confinement Effect

Quantum confinement can be observed once the diameter of a material is of the same magnitude as the de Broglie wavelength of the electron wave function. When the QD size of the particle reaches the nanometer scale, the electronic energy level near the Fermi energy level splits from the continuum to the discrete energy level, and their electronic and optical properties deviate substantially from those of bulk materials (Figure 1.3). For semiconductor materials, the size of the bandgap can be adjusted by changing the scale of the particles, thus changing the reliance on certain very costly semiconductor materials (Figure 1.4). Quantum confinement effects in QDs can also result in fluorescence intermittency, called "blinking" [4].

1.2.2.4 Quantum Tunnelling Effect

Quantum tunning effect is one of the fundamental quantum phenomena, i.e. when the total energy of a microscopic particle is less than the height of the potential barrier, considering the motion of a particle encountering a potential barrier above the energy of the particle, the particle is still able to cross this barrier, which indicates that on the other side of the barrier, the particle has a certain probability that the particle penetrates the potential barrier. For QDs, electron movement in the nanoscale space, the carrier transport process will have obvious electronic fluctuations, the emergence of quantum tunneling effect, and the energy level of the electron is discrete [5]. To achieve the quantum effect, it requires the formation of nano-conducting domain in a few μm to tens of μm tiny area. When the voltage is low, the electrons are confined to the nanoscale range of motion, and increasing the voltage can make the electrons cross the nanopotential barrier to form a sea of Fermi electrons, making the system conductive. The

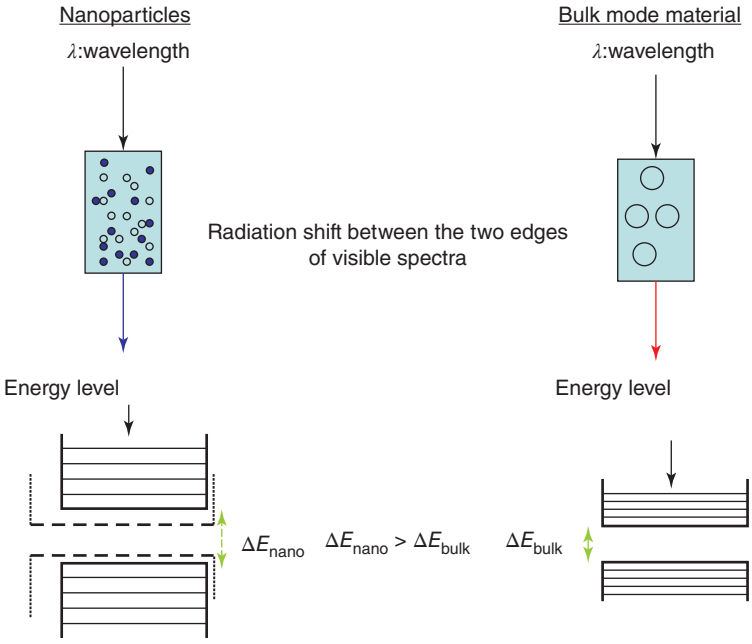

Figure 1.4 QDs Confinement effect: As the size of the particles decreases, the electrons and electron holes come closer, and the energy required to activate them increases, which ultimately results in a blueshift in light emission. Source: Adapted from Kang and Min [3].

quantum tunneling effect occurs when electrons cross the quantum barrier from one quantum well into another quantum well, and this insulating to conducting critical effect is a characteristic of the QDs in a nano-ordered array system. Most QD solids exhibit complex charge-carrier interactions between carrier confinement, interfacial properties, and quantum tunneling effects in the nature of electronic coupling [6].

1.2.2.5 Quantum Optical Properties

Owing to the above-mentioned effects of QDs, the QD absorption and emission features correspond to transitions between discrete quantum mechanically allowed energy levels in the box, which are reminiscent of atomic spectra. QDs have intermediate properties between bulk semiconductors and discrete atoms or molecules. Their optoelectronic properties change as a function of both size and shape. Larger QDs of 5–6 nm diameter emit longer wavelengths, with colors such as orange, or red. Smaller QDs (2–3 nm) emit shorter wavelengths, yielding colors like blue and green. Whereas, the specific colors vary depending on the exact composition of the QD. It turns out that QDs have broad absorption spectra, meaning that they can be excited across a pretty expansive range of light wavelengths. Figure 1.5 shows the emission color of QDs dependent on their respective sizes.

Recent studies have also shown that the shape of the QD may play a role in the band-level energy of the QD, thus affecting the frequency of fluorescence emission

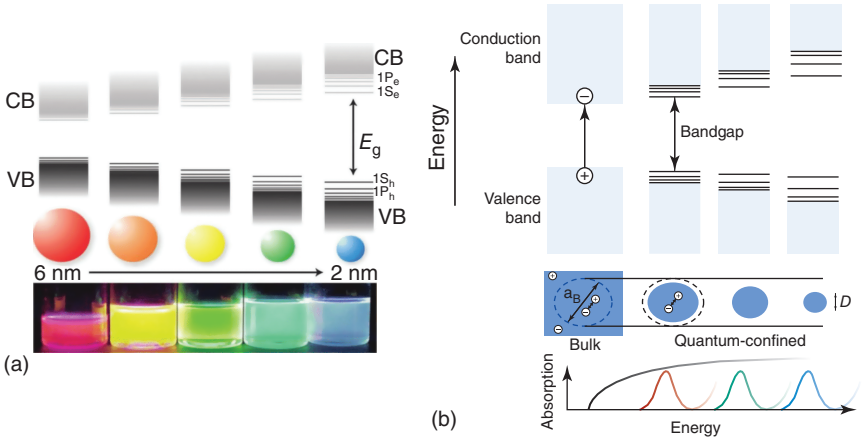

Figure 1.5 (a) Schematic representation of the quantum confinement effect on the energy level structure of a semiconductor material. The lower panel shows colloidal suspensions of CdSe NCs of different sizes under UV excitation. Source: Donegá [7]/Royal Society of Chemistry.; (b) Quantum confinement, leading to size-dependent optical and electrical properties that are distinct from those of parental bulk solids, occurs when the spatial extent of electronic wave functions is smaller than the Bohr exciton diameter. Source: García de Arquer et al. [8]/American Association for the Advancement of Science.

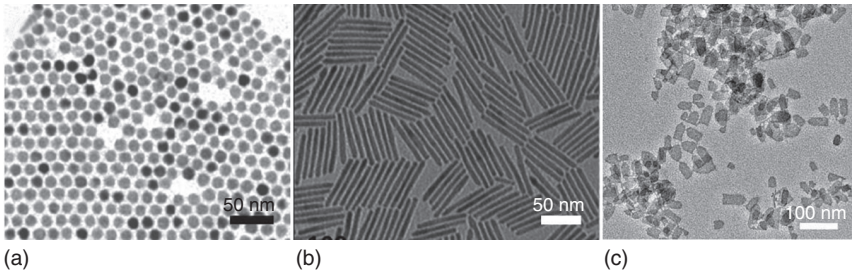

Figure 1.6 Pictures of quantum dots with various sizes and morphologies taken with transmission electron microscopy (a) quantum dots, (b) quantum rods, and (c) quantum sheets.

or absorption. The luminescence characteristics of QDs are closely related to their size and shape, the presence or absence of core–shell structure, and their surface chemistry. QDs of various sizes, morphologies, and core–shell structures can be synthesized by colloidal chemistry, as shown in the transmission electron microscope image in Figure 1.6.

The ligand type and ligand concentration on the surface of colloidal QDs also have an effect on their luminescence properties. For example, Peng et al. observed a shift of several nanometers in the peak position of the fluorescence emission peak of CdSe/CdS core–shell structured QDs ligated by fatty acid cadmium salt surface after ligand exchange treatment by aliphatic amines (Figure 1.7). The QDLED luminescence performance indexes such as external quantum yield and lifetime of CdSe/CdS core–shell QDs with different surface ligands are even more different when prepared

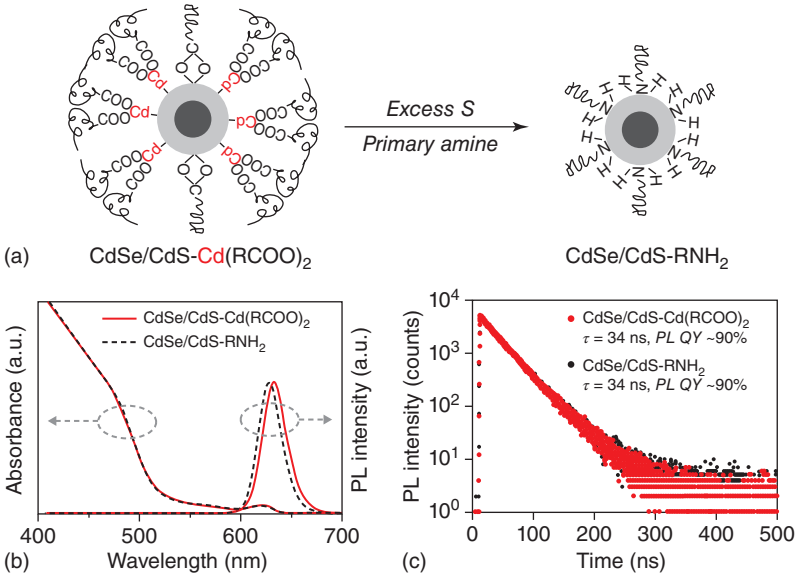

Figure 1.7 Photoluminescence and electroluminescence properties of CdSe/CdS-Cd(RCOO)$_2$ and CdSe/CdS-RNH$_2$ quantum dots. Schematic diagram of CdSe/CdS quantum dots with fatty acid cadmium surface ligands (and also a small amount of negatively charged carboxylates) undergoing ligand exchange to generate CdSe/CdS quantum dots with aliphatic amines. (b) Absorption and steady-state photoluminescence spectra. (c) Time-resolved photoluminescence spectrum with single-exponential decay lifetime (τ) and quantum yield (QY). Source: Pu et al. [9]/CC BY 4.0/Public Domain.

into QDLED devices [9]. Therefore, we should pay special attention to the surface chemical state when studying the luminescence properties of QDs.

The effect of crystal structure can also affect the emission color. Table 1.1 illustrates common bulk semiconductor physical properties. The crystal lattice of a QD semiconductor has an effect on the electronic wave function. As a result, QDs have a specific energy spectrum equal to the bandgap and a specific density of electronic states outside the crystal. Compared to conventional fluorophores, QDs have unique optical and electronic properties. Examples include high quantum yields and molar extinction coefficients, large effective Stokes shifts, broad excitation spectra, narrow emission spectra, a high resistance to reactive oxygen species, protection against material degradation, and nearly impervious to photobleaching.

In highly monodisperse colloidal QD samples, due to the quantum size effect, electrons and holes are subjected to quantum confinement effect, atomic-like structure of electronic states of QDs leads to the formation of discrete energy levels of narrow full-width at half maximum (FWHM) width of 20–80 meV at room temperature and symmetrical fluorescence emission peaks [10] (Figure 1.8).

1.2.3 Core–Shell Structure of QDs

For most core QDs, due to their low PLQYs and poor stabilities, they tend to exhibit a broad red-shifted emission, owing to the surface defects. The issues can be

Table 1.1 Common bulk semiconductor physical parameters.

Material name	Crystal structure type (300 K)	Category	E_{gap} (eV)	Lattice parameters (Å)	Density (g cm^{-3})
ZnS	Sphalerite	II–VI	3.61	5.41	4.09
ZnSe	Sphalerite	II–VI	2.69	5.67	5.27
ZnTe	Sphalerite	II–VI	2.39	6.10	5.64
CdS	Wurtzite	II–VI	2.49	4.14/6.71	4.82
CdSe	Wurtzite	II–VI	1.74	4.3/7.01	5.81
CdTe	Sphalerite	II–VI	1.43	6.48	5.87
InP	Sphalerite	III–V	1.35	5.87	4.79
GaAs	Sphalerite	III–V	1.42	5.65	5.32
PbS	Rock salt	IV–VI	0.41	5.94	7.60
PbSe	Rock salt	IV–VI	0.28	6.12	8.26
PbTe	Rock salt	IV–VI	0.31	6.46	8.22

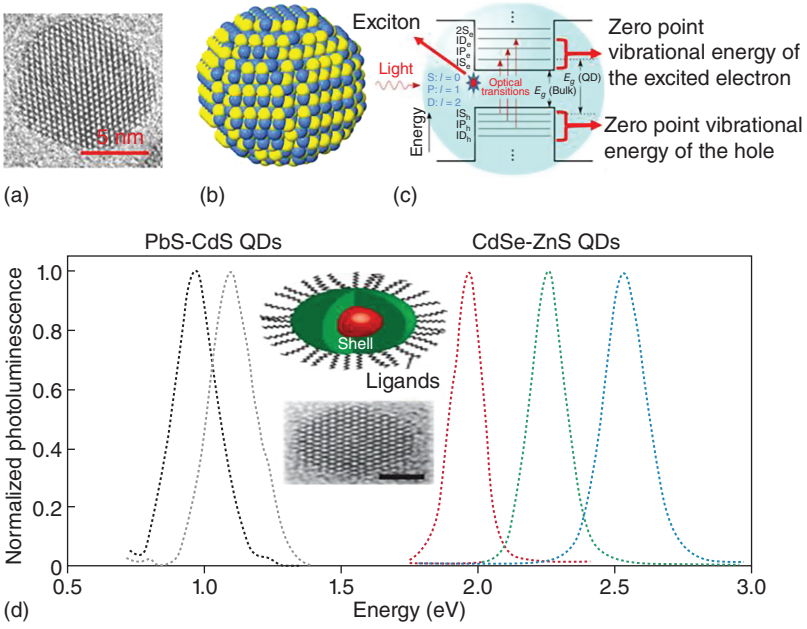

Figure 1.8 (a) TEM image of CdSe nanocrystal; (b) nanocrystal atomic structure; (c) energy level discreteness of the excited electron and the hole in an exciton entity. (d) PL spectra of CdSe–ZnS and PbS–CdS core/shell colloidal QDs. Source: Efros and Brus [2]/American Chemical Society.

addressed to improve efficiency and brightness of semiconductor NCs by growing shells of another higher-bandgap semiconducting material around them, resulting in core–shell QDs. The improvement is due to the reduced access of electrons and holes to non-radiative surface recombination pathways, and in other cases, due to the reduced Auger recombination (AR). Core–shell QDs (core@shell QDs) hold the promise of being emissive components through the precise control of shade and an improved color-rendering index. They exhibit improved optical properties over pure core-only QDs due to the growth of the shell around the QD core, which improves stability and photoluminescence efficiency. A fundamental feature of QDs is the tunability of their emission color through precise control of their size and composition, giving access to UV, visible, and near-infrared wavelengths. Continuing improvements in engineering core–shell QD structures, where a 1–10 nm binary, ternary, or alloyed semiconductor core particle is surrounded by a shell composed of one or more semiconductors of a wider bandgap, have resulted in materials with fluorescence quantum yields that approach unity, narrow symmetric spectral line shapes, and remarkable stabilities, as shown in Figure 1.9, for CdSe/ZnS QDs [11], CdSe/CdS quantum rods [12], CdSe quantum sheets [13]. Interestingly, the fluorescence emission peaks of QDs and quantum rods have a large Stocks shift with the peak position of their first exciton absorption peaks, while the fluorescence emission peaks of quantum sheets have almost no Stocks shift with the peak position of their first exciton absorption peaks. In addition, in terms of fluorescence lifetime, the fluorescence lifetime of rare-earth luminescent materials is at millisecond or microsecond level, while the fluorescence lifetime of QDs is usually in the range of milliseconds [14–16]. While the fluorescence lifetime of QDs is usually below 100 ns [17–19]. It has been found that the fluorescence emission of single QDs has severe blinking behavior, ranging from a few milliseconds to a few minutes, which is mainly due to the non-radiative compounding process caused by the "surface defects" of QDs [20–22].

Although the PL of II–VI QDs can be bright and stable under a reasonable range of excitation light intensities, core–shell QDs universally showed significant "blinking" under the high fluxes used in single QD fluorescence spectroscopy, whereby the PL of single QDs turns "on" and "off" under continuous excitation. This single QD "blinking" not only limits the use of QDs as single photon sources but also

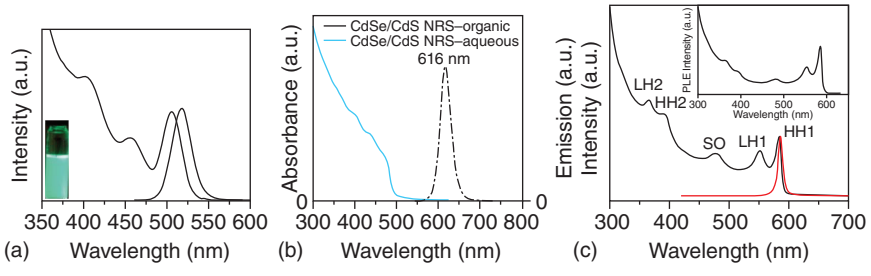

Figure 1.9 Absorption and emission spectra of (a) CdSe/ZnS quantum dots, (b) CdSe/CdS quantum rods, and (b) CdSe quantum sheets.

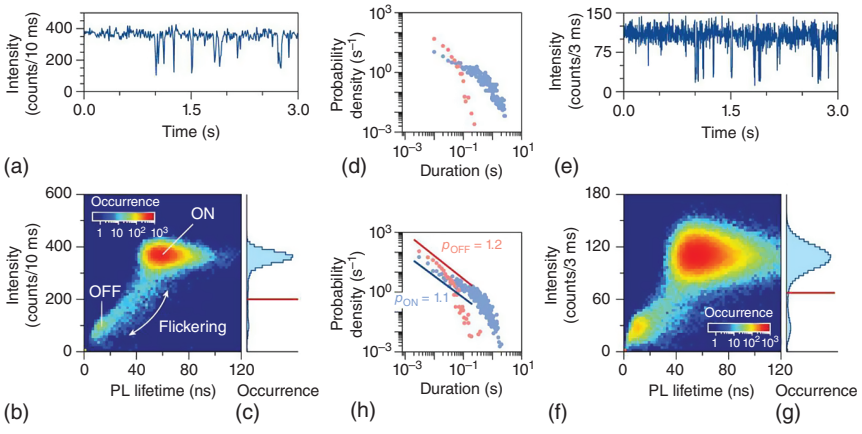

Figure 1.10 (a) Emission intensity from a single CdSe/CdS/ZnS core/shell/shell quantum dot with a temporal resolution of 10 ms under pulsed excitation (405 nm; 10 MHz; 1 μJ cm^{-2}). The diameter of the quantum dot core is 3.2 nm and the shell has 8(2) CdS(ZnS) monolayers. (b) The corresponding "fluorescence lifetime intensity distribution" is a two-dimensional histogram. The plot is based on a 300 seconds experiment, which was divided into 30 000 10 ms time intervals. The effect of scintillation is highlighted. (c) Corresponding 1D intensity histogram with thresholds used for statistical analysis indicated by red lines. (d) Flicker periods (blue) and non-flicker periods (red) extracted from the 10 ms merged and thresholded data in (a) plot. (e–h) Same as (a–d), but using the same single photon data on which there are 3 ms time bins for statistics. Source: Rabouw et al. [22]/American Chemical Society.

potentially limits QDs from being a stable photoluminescent output source under relatively high fluxes. A different approach to blinking suppression was explored by growing a thick CdS or CdS/CdZnS/ZnS shell (>5 nm in shell thickness) onto CdSe core QDs with the idea of fully isolating the excited carriers from the QD surface and the surface environment [22]. However, these QDs generally do not have a very good size distribution, exhibit broad PL spectra, and display moderate PL QYs. More recently, synthesis of CdSe/CdS QDs at a high reaction temperature (310 °C) using octanethiol as a sulfur precursor resolved many of these issues (Figure 1.10).

The terms Type I and Type II QDs are used to classify QDs based on their band structure and electron–hole recombination dynamics (Figure 1.11). Type I and Type

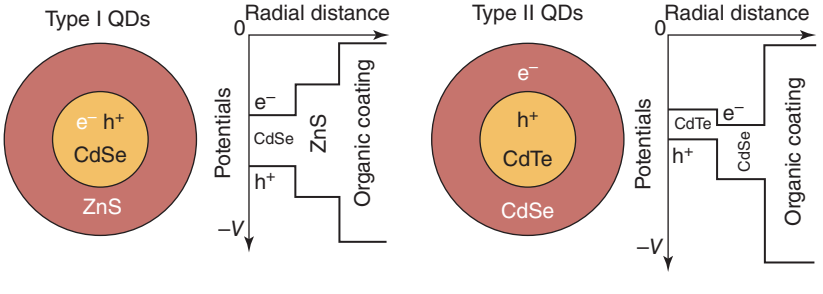

Figure 1.11 Comparison of Type I and Type II CdSe/ZnS core–shell quantum dots. Source: Vaneski [23]/Aleksandar Vaneski.

II QD materials are two different categories of semiconductor nanostructures that exhibit unique electronic and optical properties due to their quantum confinement effects. In a Type I QD, the electrons and holes are confined in the same region of the QD, resulting in a strong overlap of their wave functions. This leads to efficient radiative recombination of the electron–hole pairs, resulting in a high quantum yield and bright fluorescence. Examples of Type I QDs include CdSe, CdTe, and InP QDs. In contrast, in a Type II QD, the electrons and holes are spatially separated between two different regions of the QD due to a band offset at the interface. As a result, radiative recombination of the electron–hole pairs is less efficient than in a Type I QD, leading to lower quantum yields and longer-lived excitons. However, Type II QDs exhibit unique properties such as multiple exciton generation and efficient charge separation, which make them attractive for applications such as solar cells and photocatalysis. Examples of Type II QDs include CdS/CdTe, CdSe/CdTe, and CdSe/ZnTe QDs. Both Type I and Type II QDs have found numerous applications in areas such as optoelectronics, bioimaging, and sensing due to their unique properties and tunability.

Giant QDs are a type of QD structure that is characterized by a larger size and a more complex core–shell structure than traditional QDs. While traditional QDs typically have dimensions on the order of a few nanometers, giant QDs can have dimensions up to tens of nanometers. The larger size of giant QDs offers several advantages over traditional QDs. For example, giant QDs have a higher absorption cross-section, which allows them to absorb more light and generate more charge carriers per photon. They also have a higher quantum yield and longer emission lifetime due to reduced surface recombination and enhanced confinement of excitons. Giant QDs can be synthesized using various methods, including the core–shell approach, which involves the growth of a large core particle, followed by the deposition of multiple layers of shell material. The resulting core–shell structure can have a complex morphology, such as a core–shell–shell or a core–shell–shell–shell structure. Applications of giant QDs include bioimaging, sensing, and photovoltaics. In bioimaging, giant QDs can be used as contrast agents due to their bright and stable emission. In sensing, they can be used as probes for detecting biomolecules due to their high sensitivity and specificity. In photovoltaics, giant QDs can be used as absorbers in thin-film solar cells due to their high absorption efficiency and tunable bandgap.

1.2.4 Continuously Gradated Core–Shell Structure of QDs (cg-QDs)

For most core/shell QDs, such as giant CdSe/CdS core–shell QDs (denoted CdSe/CdS g-QDs, where the small CdSe core is passivated by the large CdS shell) synthesized by the successive ion layer adsorption and reaction (SILAR) method, exhibit reduced surface trapping and AR. Notably, this core/shell QD shows a significant redshift of the emission peak, which indicates that the CdSe core wave function extends into the CdS shell region, i.e. the effective size of the core increases. In addition, the first absorption peaks of CdSe/CdS g-QDs are relatively suppressed, which is due to the fact that the bandgap of CdS is larger than that of CdSe, so the absorption mainly comes from the thick CdS shell. However, due to the large

bandgap of CdS (e.g. 2.42 eV; corresponding to an absorption onset of 512 nm), the emission position of CdSe/CdS g-QDs achieving reabsorption suppression is limited throughout the visible region compared to CdSe. In addition, g-QDs are typically prepared by the SILAR method, which requires multiple time-consuming steps to epitaxially deposit the desired shell material. It is clearly desirable to develop alternative, simple, robust, and convenient synthetic routes to prepare g-QDs with enhanced photostability and quantum yields. It has been recently demonstrated that the implementation of larger CdSe QDs and CdSe QDs with hierarchical shell structures can reduce the AR rate. In this context, cg-QDs with smooth confinement potentials hold promise for effectively reducing nonradiative AR, such as suppressing intraband conversion of additional carriers during Auger recombination and greatly balancing the charge injection in QDLEDs brought about by the fine nanostructure of cg-QDs. These QDs with chemical composition gradients possess excellent photostability due to the judicious incorporation of CdSe/$Cd_{1-x}Zn_xSe_{1-y}S_y$ graded shells, which mitigate the lattice strain between CdSe and ZnS as shown in Figure 1.12 [24]. Furthermore, the Stokes shift (i.e. the difference between absorption and emission maxima) of these QDs with graded shell structures can be easily engineered by simply further adjusting the thickness of the outermost ZnS shell (i.e. redshift with increasing ZnS shell thickness), which is not observed in conventional CdSe/ZnS QDs because of their energy level mismatch. It is also noteworthy that CdSe/$Cd_{1-x}Zn_xSe_{1-y}S_y$/ZnS QDs are more advantageous than giant CdSe/CdS QDs because the bandgap of ZnS is larger than that of CdS and thus highly tunable due to the suppression of reabsorption when choosing the emission position in the visible region. All CdSe/$Cd_{1-x}Zn_xSe_{1-y}S_y$/ZnS

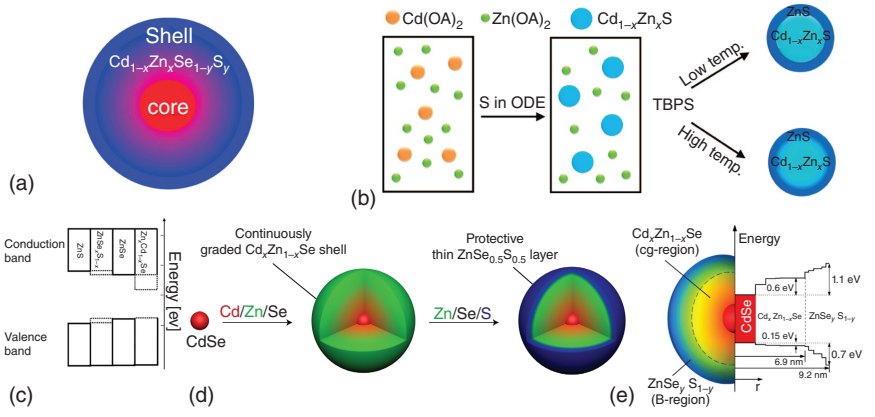

Figure 1.12 Fabrication methods of cg-QDs. (a) One-step synthesis of $Cd_{1-x}Zn_xSe_{1-y}S_y$ cg-QDs with continuously graded nanocompositions along the whole radial direction. (b) Schematic illustration of continuously graded $Cd_{1-x}Zn_xS$ cores with ZnS shell. The smoothness of the core/shell interface can be adjusted by changing the reaction temperatures during shell growth. (c) The energetic band alignments of $Zn_{1-x}Cd_xSe$/ZnSe/$ZnSe_xS_{1-x}$/ZnS QDs. (d) Reaction schematics of CdSe/$Cd_xZn_{1-x}Se$/$ZnSe_{0.5}S_{0.5}$ QDs with multistep synthesis. (e) Structures and band alignments of CdSe/$Cd_xZn_{1-x}Se$/$ZnSe_yS_{1-y}$ QDs. Source: Shen et al. [24]/American Chemical Society.

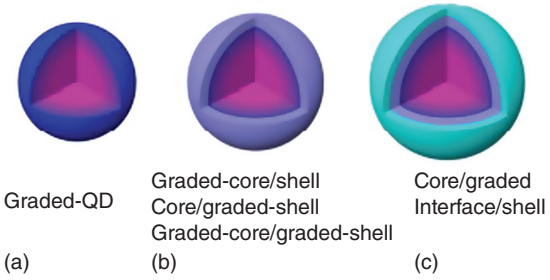

Figure 1.13 Schematics of three types of cg-QDs. (a) cg-QDs with no distinct boundary between the core and shell layers; (b) cg-QDs with one or both of the core and shell are continuously graded along the radial direction; (c) cg-QDs with continuously graded intermediate layers between the core and shell of the QD. Source: Cheng et al. [25]/American Chemical Society.

QDs with different emission positions exhibit longer lifetimes compared to ordinary CdSe QDs, which implies a reduced AR rate as a direct result of electron wave function delocalization over the whole QD.

The CdS- and CdS-based cg-QDs reported so far can be divided into three main categories: (i) QDs that are continuously graded along the entire radial direction, i.e. no distinct boundary between the core and shell layers (Figure 1.13a); (ii) QDs in which one or both of the core and shell are continuously graded along the radial direction (Figure 1.13b); (iii) continuously graded intermediate layers between the core and shell of the QD (Figure 1.13c) [25]. It should be emphasized that although unintentional alloying of the core/shell interface has been achieved in the early stages of QD synthesis, it is now possible to precisely and quantitatively control the elemental composition ratio and the thickness of the cg-QD layer. In contrast to the shell layer growth method based on continuously graded cores, another widely used technique is to grow shell layers directly on discontinuous cores, which also exhibit good optical properties. Continuously graded CdSe/$Cd_xZn_{1-x}Se$/$ZnSe_{0.5}S_{0.5}$ QDs were synthesized by Lim et al. and are expected to have great potential in DC-pumped lasers [26]. After dispersing the CdSe core in a mixed solution and controlling the constant injection of reactants, they obtained a continuously graded $Cd_xZn_{1-x}Se$ shell on the CdSe core. In addition, they coated these CdSe/$Cd_xZn_{1-x}Se$ particles with a thin $ZnSe_{0.5}S_{0.5}$ shell to protect the QDs from degradation. Lim et al. also proposed a novel multishell QD consisting of a CdSe core coated with a continuously graded $Cd_xZn_{1-x}Se$ inner shell followed by a $ZnSe_yS_{1-y}$ barrier shell. The $Cd_xZn_{1-x}Se$ inner shell is able to suppress the AR process, while the $ZnSe_yS_{1-y}$ shell with a wide gap is able to optimize electron and hole injection in QDLEDs [25].

1.2.5 Typical QDs Materials

QDs are nanoscale semiconducting materials with unique optical and electronic properties. QDs can be made from a variety of materials, including metals, semiconductors, and organic molecules. Here are some common QD materials and their properties:

Cadmium selenide (CdSe): CdSe is one of the most commonly used QD materials. It has a high quantum yield and narrow emission spectra, making it useful for a variety of applications, including biological imaging and photovoltaics;

Cadmium telluride (CdTe): CdTe has a similar bandgap to CdSe but a larger Bohr exciton radius, which makes it useful for photovoltaic applications. It is also more environmentally friendly than CdSe;

Indium arsenide (InAs): InAs QDs have a narrow bandgap, which makes them useful for infrared applications. They are also good for quantum computing and single-photon sources;

Lead sulfide (PbS): PbS QDs have a large Bohr exciton radius and can absorb light in the near-infrared region, making them useful for imaging and sensing applications;

Silicon (Si): Silicon QDs have a tunable bandgap and good biocompatibility, which makes them useful for biological imaging and sensing;

Perovskite QDs: Perovskite QDs are a new class of QDs that have recently gained attention due to their high quantum yield, tunable bandgap, and low toxicity. They have potential for use in solar cells, LEDs, and other optoelectronic devices.

These are just a few examples of many QD materials that have been developed. The choice of QD material depends on the specific application and desired properties.

Similar to the bulk semiconductor materials, typical QDs can also be classified as single-element QDs such as C and Si-based QDs (denoted as 1-D QDs), binary QDs (denoted as 2-D QDs), ternary QDs, and alloy QDs (denoted as 3-D QDs), as shown in Figure 1.14.

According to the specific structures and properties, the types of QDs can also be divided into core–shell QDs and Janus QDs. The former refers to a central core surrounded by a shell, while the latter refers specifically to a core with two different material "halves."

Core–shell QDs are nanoscale semiconductor materials that have a core of one material surrounded by a shell of another material. The core of the QD typically consists of a semiconductor material with a small bandgap, such as CdSe or PbS, while the shell is made up of a material with a wider bandgap, such as ZnS or CdS.

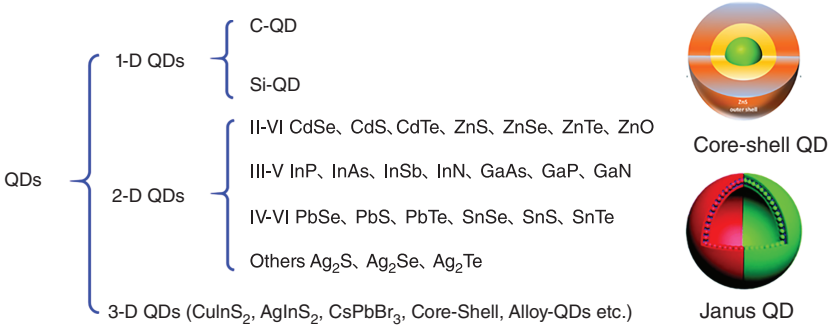

Figure 1.14 Classification of QDs based on composition type and structure type.

The core–shell structure of QDs provides several advantages over simple core–only QDs. First, the shell material can act as a barrier to prevent the diffusion of impurities into the core, which can degrade the optical properties of the QD. Second, the shell can provide additional stability to the QD by preventing oxidation and protecting the core from environmental degradation. Third, the shell can modify the electronic properties of the QD, such as the exciton energy and electron–hole recombination rate, which can improve the photoluminescence efficiency of QD and make it more suitable for various applications in optoelectronics and biological imaging. Core–shell QDs have shown great potential in a wide range of applications, including bioimaging, light-emitting diodes, solar cells, and single-electron transistors.

Janus QDs are a type of QD with a core–shell structure, where one half of the shell is made of one material and the other half is made of a different material. The name "Janus" refers to the two-faced Roman god, who is often depicted with two different faces looking in opposite directions. Janus QDs can have a number of interesting properties, such as asymmetric surface charge distributions, anisotropic shapes, and tunable surface properties. These properties make Janus QDs attractive for a range of applications, including catalysis, sensing, and imaging. Janus QDs can be synthesized using a number of methods, including co-precipitation, SILAR, and reverse micelle methods. The choice of synthesis method can impact the properties of the resulting Janus QDs, such as their size, shape, and composition. Janus QDs are an exciting area of research with potential for a wide range of applications due to their unique properties and versatility in synthesis.

1.2.5.1 II–VI Semiconductor QDs

Semiconductor QDs of the II–VI family, especially those based on CdSe, exhibit a tunable band-edge emission covering the visible spectrum (480–650 nm). They have been the most extensively investigated QDs and are recognized as a model system. The full range of visible colors from emissive II–VI QDs has given rise to a series of images as shown in Figure 1.15a, highlighting the color tunability of core–shell QDs. Figure 1.15b illustrates the bandgap of the bulk semiconductors.

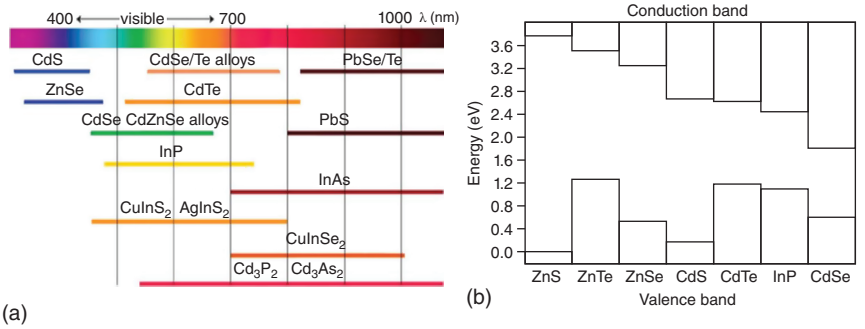

Figure 1.15 (a) Reported spectral range of emission for different semiconductor quantum dots. (b) Bandgap of the bulk semiconductors.

1.2.5.2 IV–VI Semiconductor QDs

Lead chalcogenide IV–VI semiconductor QDs are characterized by their tunable NIR emission from 600 to 2200 nm. PbSe and PbS NCs are widely explored including, the development of core–shell PbSe/CdSe and PbS/CdS QDs. These QDs exhibit intrinsically strong quantum confinement and have seen deep interest in various applications such as photodetectors, LEDs, and photovoltaic solar cells.

1.2.5.3 II_3–V_2 Semiconductor QDs

II_3–V_2 semiconductor QDs (e.g. Cd_3P_2 and Cd_3As_2) with efficient PL have only been reported very recently. Cd_3As_2 QDs with emission in the NIR range have the highest QY of 85%, an average size of 2.5 nm, and an emission wavelength of ~900 nm. Good-quality core–shell QDs for this class of NIR- and IR-emitting QDs would enhance their properties and are lacking thus far.

1.2.5.4 Ternary I–III–VI_2 Chalcopyrite Semiconductor QDs

Ternary semiconductor QDs such as the I–III–VI_2 chalcopyrites $CuInSe_2$ (CISe) and $CuInS_2$ (CIS) have emerged in the past few years as further alternative materials to cadmium-based systems without toxic elements. They are direct semiconductors and exhibit a relatively narrow bandgap (1.05 eV for CISe, 1.5 eV for CIS). Ternary CISe and CIS QDs were mainly studied because of their potential use in photovoltaics.

1.2.5.5 Single Element-Based Semiconductor QDs

In recent years, many studies on single-element QD materials in nonlinear optics and ultrafast lasers have been reported, such as graphene QDs, carbon QDs, black phosphorus (BP) QDs, sulfur QDs, silicon QDs, selenium QDs, boron QDs, and metal elemental QDs. In recent years, the interest has been in C-QDs and Si-QDs [27]. Carbon quantum dots, also commonly referred to as carbon dots (abbreviated as CQD), are carbon nanoparticles less than 10 nm in size with surface passivation possibility. As a new class of fluorescent carbon nanomaterials, CQD has high stability, good electrical conductivity, low toxicity, environmental friendliness, simple synthesis routes, and optical properties comparable to QDs. Most CQD research applications are in the fields of chemical sensing, biosensing, bioimaging, nanomedicine, photocatalysis, and electrocatalysis [28].

Silicon QDs are metal-free, biocompatible quantum dots with photoluminescence emission peaks that can be modulated from the visible to near-infrared spectral regions. These QDs have unique properties due to their indirect bandgap, including long-lived luminescent excited states and large Stokes shifts. Silicon quantum dots (SiQDs) have size-tunable photoluminescence similar to that observed for conventional QDs. By varying the size of the Si QDs, the LED emission can be tuned from deep red (680 nm) to orange/yellow (625 nm), although Si QDs-LEDs exhibit low efficiency and broad luminescence emission that can be improved by further studies [29].

1.3 Application of Quantum Dots on Display Devices

As QDs have adjustable emission peaks, high color purity, and high photoluminescence quantum yield, they have attracted more and more attention in academia and industry, and have now been commercially used in LCD backlight products [30, 31]. For white LED products in traditional LCD backlighting, yellow phosphor is used for down conversion, and its color gamut range only reaches 70% of the National Television Standards Committee (NTSC) standard [32]. While products with QDs as backlight can achieve high saturation and a color gamut greater than 100% of the NTSC standard. At present, Samsung, TCL, BOE, and other domestic and foreign display panel manufacturers have adopted QDs as the backlight technology solution for high-end display panels.

Compared to other display technologies such as LED-backlit LCDs and OLEDs, the design and manufacture of quantum dot light-emitting diodes (QDLEDs), which are directly driven by voltage, has greater appeal and development potential in terms of display technology specifications such as contrast, color gamut, response time, and viewing angle. In addition, QDLEDs have better temperature and moisture resistance than OLEDs and have better application prospects in the field of flexible devices.

1.3.1 The Basic Structure of QDLED

The schematic diagram of QDLED device structure is shown in Figure 1.16, which is a typical sandwich structure with multiple functional layers stacked together, in which indium tin oxide (ITO) material is used as the anode, s-NiO material as the hole transport layer, Al_2O_3 material as the electron blocking layer, QD light-emitting

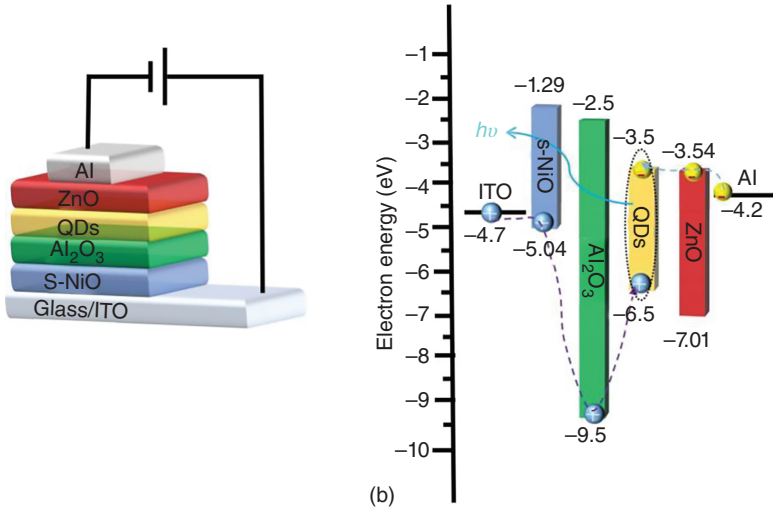

Figure 1.16 Basic structure of QDLED: (a) schematic diagram of QDLED device structure, (b) schematic diagram of energy level of each functional layer of QDLED device.

material as the light-emitting layer, ZnO material as the electron transport layer, and Al material as the cathode. In QDLED, after passing voltage, electrons and holes are transferred from the cathode and anode to the QD light-emitting layer, respectively, and combine in the light-emitting layer to form electron–hole pairs (excitons) to produce photons. In addition, the electron-blocking layer composed of Al_2O_3 material is also required to assume the charge-blocking role to improve the luminescence efficiency of the QDLED device. The LUMO/conducting band bottom of the hole transport layer needs to be shallow enough for hole transport; the HOMO/valence band top of the electron transport layer needs to be deep enough for electron transport.

1.3.2 Main Factors Affecting QDLED Light Emission

The main challenge for QDLED commercialization is that active matrix QDLED (AM-QDLED) devices are difficult to achieve relatively high luminous efficiency and up-to-standard lifetime [33]. The main factors affecting their performance include charge carrier combination, fluorescence resonance energy transfer, and field effect quenching. The prerequisites for high external quantum efficiencies (EQEs) are a high PLQY and good balance between electron and hole injection currents to avoid CQD charging because the formation of charged excitons promotes nonradiative AR. During Auger decay, the electron–hole recombination energy is not released as a photon but instead transferred to the resident charge carrier. AR has been identified as at least one of the reasons for EQE droop – a decrease in device efficiency with increasing current density (Figure 1.17). Compositionally graded QD multishell heterostructures have been shown to impede AR because of creation of a "smooth" confinement potential that suppresses the intragap transition involving the energy-accepting carrier and thus minimizes the efficiency roll-off [35].

1.3.2.1 Auger Recombination (AR)

When an electron is excited to a higher energy level by a photon, a hole is created at the same time, forming an electron–hole pair; and when the electron–hole pair recombines, a photon is emitted. The recombination dynamics of these single

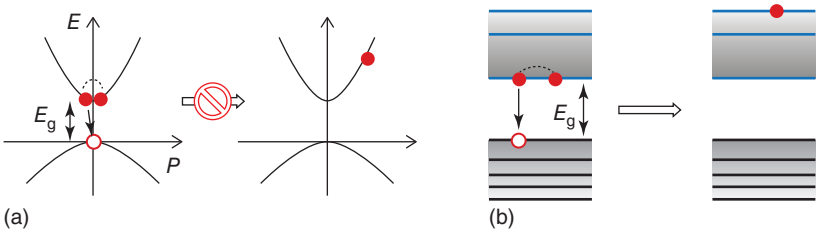

Figure 1.17 (a) In a bulk semiconductor, at $T = 0$ when the kinetic energies of all three charge carriers are zero, Auger recombination is not possible, as it violates translational momentum conservation. (b) In QDs, translational momentum conservation is relaxed, resulting in efficient Auger recombination even at $T = 0$. Source: Pietryga et al. [34]/American Chemical Society.

excitons in well-passivated QDs are dominated by intrinsic radiative recombination. The situation dramatically changes in the case when one or more extra carriers are introduced into the NC (for example, at higher current densities), which opens a new nonradiative pathway associated with AR. However, the energy can be directly transferred to the third carrier in this process, which is called AR, if a third carrier is present [36, 37]. In this process, the recombination energy of the e–h pair is not converted into radiation but instead is used to excite a third charge carrier (an electron or a hole) into a higher energy level [34]. In bulk materials, the AR is hindered because the conservation of energy and momentum leads to a threshold that limits the rate of AR (Figure 1.17a). In QDs, however, momentum conservation is relaxed, especially in strongly confined regions such as interfaces or defect sites. Therefore, QDs usually have efficient AR (Figure 1.17b).

In bulk semiconductors, due to the requirement of simultaneous conservation of energy and flat mobile quantities, AR is a temperature-activated process whose rate can be expressed as $r_A \propto \exp(-\gamma_A E_g/k_B T)$, where γ_A is a constant dependent on the electronic structure of a particular semiconductor. Based on this expression, the rate of Auger decay quickly decreases with increasing bandgap. As a result, AR is considerably less efficient in bulk wide-gap (e.g. CdSe and CdS) compared to narrow-gap (e.g. PbSe and PbS) materials. However, in QDs subject to strong spatial constraints, the translational momentum conservation is relaxed and replaced by a less stringent angular momentum conservation, making the AR in QDs unusually strong. The AR process is highly dependent on the size of the QDs [38]. Although there are different paths for the AR process in direct and indirect bandgap semiconductors, the increase or decrease of the volume can be applied to QDs with direct and indirect bandgap structures. In the former case, AR is a three-particle process, while in the latter case, photons require additional emission or absorption to satisfy momentum conservation. Relevant calculations also predict this size-dependent AR [39]. Auger decay rates of multiexciton states are expected to progressively increase with the number of charge carriers in a QD due to the increase in both the number of recombination pathways shown in Figure 1.18. The simplest form of multicarrier states in a QD is

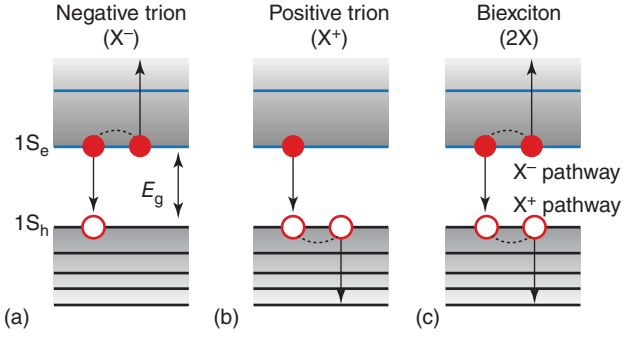

Figure 1.18 Auger recombination of (a) a negative trion (X^-), (b) a positive trion (X^+), and (c) a biexciton (2X). The energy released during e–h recombination is transferred to an electron for X^- or to a hole for X^+. In the case of biexciton Auger recombination, the energy of the e–h pair can be transferred to either an electron (X^- pathway) or a hole (X^+ pathway). Source: Pietryga et al. [34]/American Chemical Society.

a charged exciton composed of one exciton plus an extra electron or hole, which is referred to as a negative (X^-) or a positive (X^+) trion, respectively. The nonradiative Auger process is also the dominant recombination mechanism of a biexciton, which is a neutral state consisting of two e–h pairs.

AR is also related to the scintillation of QDs. The scintillation phenomenon of QDs, also known as fluorescence intermittency, is a random switch between the strong emitting state (ON) and the dark emitting state (OFF). This phenomenon has been studied by many research groups, different theoretical models have been developed and attempts have been made to explain this physical phenomenon using theoretical models [20, 40, 41]. One of the most widely accepted theories is the charge/discharge model, which attributes the scintillation to excess carriers that cause a radiation-free oscillatory process that affects the overall emission [42]. However, this model has also been challenged in some studies where size effects were not found to exist [43] and cannot explain the ultrafast nonradiative combination [44, 45]. The physical mechanism of the oscillation process and scintillation needs to be further investigated, and therefore the oscillation mechanism of the device efficiency decrease needs to be further explored.

Since the charge imbalance is expected to increase with the applied voltage, the deleterious effect of Auger decay should also increase. Therefore, AR of charged QDs has been used to explain the so-called efficiency "drop" or "roll-off" phenomenon, i.e. the decrease in EQE at higher currents typically observed in QDLEDs. These considerations suggest that the optimization of QDs applied in QDLEDs may involve not only the improvement of their single-exciton PLQYs but also the yield of charged and multi-exciton states, the latter of which can be achieved by developing methods to reduce AR.

1.3.2.2 Fluorescence Resonance Energy Transfer

The exciton energy is transferred to the defect state and the third carrier during the OSI combination process, while the exciton energy is transferred to the other radiative state during the fluorescence resonance energy transition [45]. In hybrid organic/colloidal QDLEDs, excitons are formed in organic molecules around the QD film, and exciton energy is transferred to the QDs by resonance. In addition to this layer-to-layer exciton energy transfer, there is another phenomenon of fluorescence resonance energy transfer between dots, which leads to the so-called "self-quenching" [46].

The fluorescence resonance energy transfer is influenced by the distance, so that its effective range is at the nanometer level. By assuming that the QDs are uniformly distributed, the distance between the dots can be calculated. Whereas in the solid state, the luminescent layer is usually a closed film of QDs. Since the average face-to-face distance between dots, in a QD film is usually within an energy transfer window, this structure facilitates fluorescence resonance energy transfer. Exciton diffusion among QDs within EMLs can also be responsible for efficiency losses in QDLEDs. This means that excitons can diffuse in QD films by: (i) nonradiative Forster resonant energy transfer (ET), with an efficiency that varies with dot-to-dot distance, d, as $\sim d^{-6}$; or (ii) reabsorption of emitted photons by neighboring QDs with

a rate varying as $\sim d^{-2}$. Exciton diffusion intensifies the contribution to emission efficiency loss of fast nonradiative trapping, even if this occurs only in a minority of QDs.

Traditional fluorescence electrophoresis studies using organic, biological, or inorganic materials as donors or acceptors in solution are also referred to as homogeneous transfer. In homogeneous transfer, the energy transfer process occurs between the same materials [47]. Primitive QD energy transfer studies have shown that a recognizable redshift is produced in the emission spectrum, which implies a transfer of electronic energy [48]. Due to the inhomogeneous size distribution of the QDs, the non-radiative energy transfer leads to a burst of blue luminescence and enhanced red luminescence; this results in an overall redshift in the emission spectrum. Related theoretical calculations investigated the effect of size distribution on the spectral shape and found that the increase in size nonuniformity leads to an increase in spectral shift and spectral narrowing. It has also been reported that the fluorescence resonance energy transfer process may contribute to the self-bursting of fluorescence in QDLEDs [49]. Although the so-called reduction of self-burst is associated with an increase in the inter-dot spacing, the potential mechanism of the grating contribution to the reduction of quantum efficiency remains uncertain.

1.3.2.3 Surface Traps and Field Emission Burst

For a singly excited QD, nonradiative losses are dominated by recombination at structural defects that are most often associated with the QD surface. Typically, a continuous decrease in EQE is observed in many types of QDLEDs as the current density increases, a phenomenon known as efficiency roll-off or efficiency degradation [50]. Some studies have specifically measured the efficiency roll-off of the EQE at current density. Longitudinal studies of efficiency roll-off typically quantify a range of devices by comparing parameters such as critical current density or critical luminance, and the fitted trends show that it is difficult to achieve the desired relationship between efficiency and luminance.

To understand the cause of efficiency roll-off in QDLEDs, Shirasaki et al. utilized an intelligent device design [51]. It was shown that electric fields alone can contribute to efficiency roll-off and that the drop in EQE can be predicted using a quantitative approach. Their idea builds on the relationship between the offset and intensity of the field-related spectrum. After considering the contributions of charge leakage and charge-induced Osher combinations, they propose that high field strength is a major factor in the drop in QDLED luminescence efficiency. By applying an anti-deflection field while other factors are kept constant. They observed the emission spectra at different electric field strengths and then measured the energy transfer of the emitted photons and compared them with the luminescence intensity at different bias voltages. By analyzing transient fluorescence emission spectra, they concluded that the reduced emissivity could be the cause of the efficiency roll-off.

1.3.3 History of QDLED Development

At the end of the twentieth century, few people were optimistic about the application prospects of QDLEDs because they showed only very low EQE in the early days of

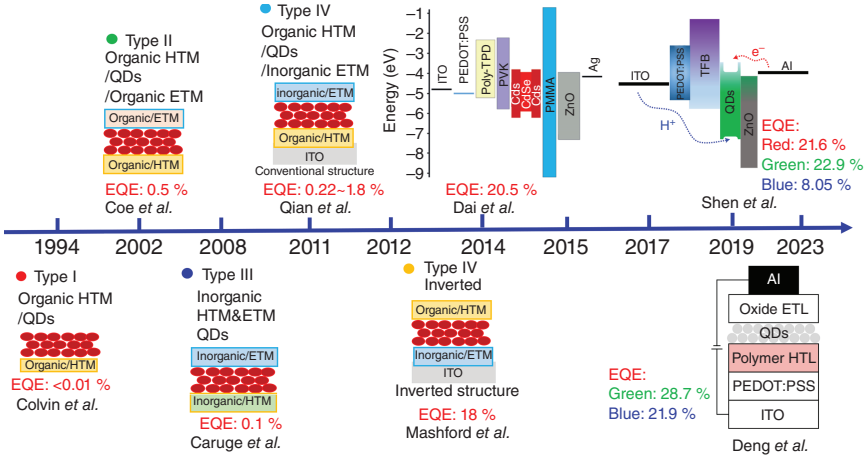

Figure 1.19 Outlines the technological development of QDLEDs in recent years (1994–2023).

electroluminescent displays. However, with the gradual maturation of OLED technology after 2000, the development of QDLEDs was inspired by the optimization of OLED structures and the working mechanisms. Since then, QDLED technology has developed rapidly, and its performance has been improving, approaching the requirements for commercial applications. In order to have an intuitive understanding of the development process of QDLED display technology, we will then briefly introduce some representative technological breakthroughs and innovative ideas in the development of QDLED display technology. It is worth noting that the continuous innovation and performance improvement of QDs and charge transport layer materials play a crucial role in the development of QDLED display technology.

The technology road map development of QDLED is illustrated in Figure 1.19. The first time reported QDLED (Type I QDLED: Organic HTM) based on a bilayer structure consisting of hole transport polymer PPV and CdSe NC active layers was reported in *Nature* by Alivisatos et al. in 1994 [52]. In 1995, the research group at MIT reported a single-layer CdSe-QDLED with the NCs incorporated into thin films ~1000 Å of polyvinylcarbazole PVK and an oxadiazole derivative *t*-Bu-PBD and sandwiched between ITO and Al electrodes. These devices exhibited very small values of EQEs of 0.001–0.01% and 0.0005%, though the room-temperature electroluminescence (EL) is nearly identical to the PL, with the same peak positions and similar linewidths. Because of the low conductivity of the organic matrix, and the poor conduction through QD multilayers led to an injected charge imbalance, the driving voltage is very high starting at 17 V, and consequently, the luminescence efficiency of these early devices never exceeded 0.10 cd A^{-1}, and considerable parasitic polymer-related emission observed in addition to QD emission [53].

The deficiencies of these devices likely originated from the charge imbalance, which led to the formation of charged excitons decaying not by radiative processes but by nonradiative AR (see Section 11.3). In the early twenty-first century, inspired by the design of OLED device structures, Coe et al. demonstrated a QDLED device

with an OLED-like device structure, in which some organic materials used in OLED devices were employed as the electron transport layer and hole transport layer materials for QDLED devices (Type II QDLED: Organic HTM and ETM), where a single monolayer of QDs was sandwiched between two organic thin films via phase segregate between the QD aliphatic capping groups and the aromatic organic materials during the spinning process, which allowed them to produce a well-defined EML/HTL bilayer and helped regulate the electron flow into the QDs. This hybrid light-emitting diode QDLED showed a 25-fold improvement in luminescence efficiency (1.6 cd A^{-1} at 2000 cd m^{-2}) over the best previously reported QDLED at that time. The application of organic materials as charge transport layer materials and the formation of QD monolayers are believed to be responsible for the increased device efficiency. In this type of QDLED devices, exciton formation is mainly achieved by the Forster resonance energy transfer (FRET) process, which is very different from direct charge injection [10]. For the FRET process, excitons are first formed in the donor electron transport layer, and then the exciton energy is transferred to the QDs via non-radiative dipole-dipole coupling. Due to the decoupling of the emission process from the charge transport, such QDLED devices can obtain an EQE of 0.5–5% [3]. Despite the considerable progress in device performance achieved with all-organic CTLs, peak EQE was still far below the theoretical limit of ~20%, determined by optical outcoupling. Imbalanced charge injection remained a significant factor; the band positions of traditionally used organic materials are not ideally suited for CdSe-based QDs. Specifically, the large offset from the LUMO of typical organic ETLs and the QD conduction band edge means that electron injection is strongly energetically favorable, even without an applied bias. At the same time, holes in the same all-organic device structure face an energetic barrier in transiting from the HTL to the QDs, requiring a significant overpotential. The prevalence of the electron-over-hole injection current leads to an excess number of electrons in the emitting layer. The resulting negatively charged dots are then susceptible to nonradiative AR, thus lowering the overall EQE. The reason for the difficulty in improving the efficiency of such devices is the difficulty in achieving a tightly packed pinhole-free monolayer to prevent carrier leakage through the QDs. In addition, the low conductivity of organic materials limits the carrier's injection [54].

A drawback to the above-mentioned device is the utilization of the organic charge support layers in QDLEDs, which creates an unwanted contribution to the light emission of the device. To overcome this, the use of inorganic charge transport materials as both hole and electron transport materials comprise an inorganic metal oxide semiconductor such as the ETL and an inorganic semiconductor such as the HTL. This new design idea for QDLED structures is realized by replacing organic charge transport layer materials with inorganic materials. According to Caruge's study, sputtered zinc oxide, tin oxide, and nickel oxide can be used as n-type and p-type charge transport layer materials, respectively. Due to the superior conductivity of metal oxides over organic transport materials, these inorganic QDLED devices (Type III QDLED: inorganic HTM and ETM) all exhibit high current densities up to 4 A cm^{-2}. However, the luminescence efficiency is low (EQE < 0.1%) due to damage to the QD layer during the sputtering of the upper layer of ZnO:SnO_2 and

insufficient hole injection due to the excessive barrier between NiO_x and QDs. In addition, exciton dynamics studies show that charge transport between QDs and adjacent metal oxides tends to occur spontaneously, leading to exciton bursts and lower device efficiency [55]. However, such all-inorganic QDLED devices are still attractive because the excellent inherent stability of metal oxides contributes to the device's lifetime. In addition, with the development of sol–gel method and NC synthesis, solution-processed metal oxides can reduce the damage to the underlying QDs. The brightness of the device was comparable to that of a Type-II device, albeit suffering from the relatively low efficiency attributed to additional quenching by the free carriers in the $ZnO:SnO_2$ ETL, yet with the benefit of improved shelf-life robustness inherent in the environmental stability of metal oxide charge transport layers [56]. The great progress was achieved using all-solution-processed QDLED device of Type IV structure consisting of a quantum dot emissive layer sandwiched between an organic hole transport layer and an electron transport layer of ZnO nanoparticles. The design of hybridized structures (Type IV QDLED: Organic HTM and Inorganic ETM) of inorganic electron transport material layers and organic hole transport material layers has been a hot research topic in the field of QDLED devices in the last decade in order to exploit the high conductivity of n-type metal oxides and the superior hole transport capability of organic materials [57–59]. In 2011, Qian et al. introduced full solution-processed QDLEDs based on ZnO nanoparticle electron transport layer materials. the resulting red, green, and blue (R/G/B) QDLEDs showed good performance with EQE peaks of 1.7%, 1.8%, and 0.22% and maximum luminance of 31 000, 68 000, and 4200 cd m^{-2} [60]. Moreover, with the incorporation of the ZnO nanoparticles as ETM, these unencapsulated devices have operating lifetimes exceeding 250 hours in low vacuum with an initial brightness of 600 cd m^{-2}. Since then, due to the advantages of high mobility, suitable electronic structure, and simple synthesis process, ZnO nanoparticles have been widely used as electron transport layer materials in QDLEDs, which has led to a leap forward in the performance of QDLED devices [4]. Under this hybrid structure, the inverted QDLED devices with QDs using ITO cathodes at the bottom reached a record of 18% EQE, which greatly exceeded the previous research results [3]. In 2014, Peng et al. achieved the first high-efficiency hybrid QDLED device (ITO/PEDOT:PSS/poly-TPD/PVK/QDs/ZnO/Ag) with an EQE of more than 20% by using a poly(methyl methacrylate) (PMMA) insulating electron blocking layer between the QD emitting layer and the ZnO electron transport layer. Since then, the improvement of the charge transport layer has received increasing attention and is considered as one of the effective strategies to achieve high-performance QDLED devices [61]. The improvement of the charge transport layer has since received increasing attention and is considered as one of the effective strategies to achieve high-performance QDLED devices.

In addition to the development of charge transport materials and modulation of device structures, it is necessary to prepare high-quality QDs by carefully controlling their nanostructure and composition in order to achieve high-performance QDLEDs. Through the fine-tuning of nanostructure of QDs, especially the composition of the graded intermediate shell and the thickness of the outer shell,

Qian et al. designed and synthesized QDs with a graded, alloyed intermediate shell ($Cd_{1-x}Zn_xSe_{1-y}S_y$) sandwiched between the Cd- and Se-rich core and the Zn- and S-rich outer shell QDs. They have successfully fabricated a full series of blue, green, and red quantum dot-based light-emitting devices (QDLEDs) with solution process, all with high external quantum efficiencies over 10%. The devices have maximum current and external quantum efficiencies of 63 cd A^{-1} and 14.5% for green QDLEDs, 15 cd A^{-1} and 12.0% for red devices, and 4.4 cd A^{-1} and 10.7% for blue devices, all of which are well maintained over a wide range of luminance from 100 to 10 000 cd m^{-2}. More importantly, the device half-lifetimes for the green and red QDLEDs showed over 90 000 and 300 000 hours, respectively, for a brightness of 100 cd m^{-2}, although the blue QDLEDs still has a relatively short lifetime of only 1000 hours. These QDLEDs also feature extremely low turn-on voltages (1.5–2.6 V), narrow full-width at half maximum (FWHM of <30 nm) of the EL peaks, highly saturated pure colors, and high brightness [62].

By incorporating ZnO NPs as the electron transport layer, and highly controlled QD synthesis, Manders et al. reported in SID 2015 the colloidal quantum dot-based hybrid light-emitting diodes (QDLEDs), which exhibited high maximum current and power efficiency of 6.1 cd A^{-1} and 5.0 lm W^{-1} for blue, 70 cd A^{-1} and 58 lm W^{-1} for green, and 12.3 cd A^{-1} and 17.2 lm W^{-1} for red emissions. It was the first time to achieve a green QDLED with EQE over 20% (21%) and 82 cd A^{-1}. These peak efficiencies occurred at a desirable luminance of 1000 cd m^{-2} and low voltage of 3.5 V [63]. High-efficiency blue CdSe/ZnS QDs were reported in 2017. Using small-size ZnO NPs, the authors have obtained a maximum current efficiency (CE) of 14.1 cd A^{-1} and a maximum EQE of 19.8 % for QDLEDs with an EL peak at 468 nm, with the CIE 1931 color coordinates (0.136, 0.078) [64]. Most previous work has focused on CdSe-based QDs, which present severe toxicity and environmental issues. To improve the operating stability of the devices and to replace their toxic cadmium composition with a more environmentally benign alternative QD, a uniform indium phosphide (InP)-based materials core and a highly symmetrical core/shell QD exhibit narrow FWHM; 35 nm at 630 nm with a quantum yield of approximately 100% was developed by Samsung Group. The device based on InP/ZnSe/ZnS QDs showed a theoretical maximum EQE of 21.4%, a maximum brightness of 100 000 cd m^{-2}, and an extremely long lifetime of a million hours at 100 cd m^{-2}. The InP-based QDLEDs will aid in fabricating Cd-free QDLEDs for next-generation displays [65].

Efforts have been made to improve the efficiency and lifetime of QDLEDs. In 2019, Shen et al. used a "low-temperature core and high-temperature shell growth" synthesis method to synthesize CdSe/ZnSe core/shell QDs and applied Se throughout the core/shell region in the presence of an alloy bridging layer at the core/shell interface, resulting in balanced charge injection and high current density at low voltage. As a result, QDLEDs based on CdSe/ZnSe core/shell structures for red, green, and blue quantum dot light-emitting diodes (ITO/PEDOT-PSS/TFB/QDs/ZnO/Al) showed maximum external quantum efficiencies of 21.6%, 22.9%, and 8.05% with corresponding luminances of 13 300, 52 500, and 10 100 cd m^{-2}. The peak luminance of these devices was also 356 000, 614 000, and 62 600 cd m^{-2}. This work represents

a significant step forward in the realization of QDLEDs for display and potential lighting applications [66].

Near-infrared NIR–QD light-emitting diodes with an EQE of 16.98% and a power conversion efficiency of 11.28% at wavelength 1397 nm have recently been reported. The authors employed a binary emissive layer consisting of silica-encapsulated silver sulfide ($Ag_2S@SiO_2$) QDs dispersed in a cesium-containing triple cation perovskite matrix that serves as an additional passivation medium and a carrier supplier to the emitting QDs. Assisted by the hole-injection thin porphyrin interlayer, which balances the device current and enhances carrier radiative recombination, The IR–QDLEDs deliver an enhanced device performance. The present approach paves the way for the development of all-solution-processable, low-cost, high performance, and large-area NIR-II light sources for biomedical and imaging applications [67].

By using deep HOMO hole transport polymers with both low electron affinity and reduced energy disorder to eliminate electron leakage at the organic/inorganic interface, the authors demonstrate green and blue QDLEDs with approximately 100% conversion of the injected charge carriers into luminescent excitons, resulting in devices that exhibit high EQE over a wide range of luminance values (green with a peak EQE of 28.7% and blue with 21.9%) and excellent stability (inferred T_{95} lifetime of 580 000 hours for green and 4400 hours for blue QDLED). The elimination of charge leakage channels may inspire other designs of solution-processed QDLEDs with organic/inorganic interfaces [68].

1.4 Conclusion and Remarks

QDLEDs offer several promising features, such as size-dependent emission wavelengths, narrow emission spectrum, high efficiency, flexibility, and low-processing cost of organic light-emitting devices. QDLEDs not only reduce the consumption of energy but also show high color purity. It exhibits the ability to be more than twice as power efficient as OLEDs at the same color purity and has also presented a 30–40% luminance efficiency advantage over OLEDs for the same color point.

Semiconductor QDs offer a great opportunity in optical electronics because of their nanometer scale size in all three dimensions, the restricted electron motion and quantum confinement effects lead to a discrete atom-like electronic structure and size-dependent energy levels. These features enable us to design nanomaterials with widely tunable light absorption, bright emission, and narrow-band pure colors. Because of the quantum size and surface effects, which provide much opportunity for control over electronic transport, and a wide tuning of chemical and physical functions benefits the applications in optical electronic devices. Specifically, the bright and narrowband light emission feature of semiconductor QDs, with tunable capability across the visible and near-infrared spectrum is attractive to realize more efficient displays with purer colors in future. In addition, the advent of colloidal QDs, which can be fabricated and processed in solution at mild conditions, enabled large-area manufacturing and widened the scope of QD applications to QDLED

display and lighting markets because QDLEDs present an ideal blend of high brightness, efficiency with long lifetime, flexibility, and low-processing cost of solution process.

Although much progress has been made, several factors limit the performance of QDLEDs, including AR, FRET, and field quenching (FIQ). In addition, most of the research and development efforts have been focused on cadmium-based QDs, which also limits their further commercialization. Therefore, the development of cadmium-free QDLEDs has high demands for their wide and practical implementation. In Chapter 2, the basic principle of QDLED, the materials and device development of QDLEDs, and a summary and perspective concerning the issues and limitations of the applicability of QDLEDs are presented.

References

1 Sun, Y., Jiang, Y., Sun, X.W. et al. (2019). Beyond OLED: efficient quantum dot light-emitting diodes for display and lighting application. *Chemical Record* 19 (8): 1729–1752.

2 Efros, A.L. and Brus, L.E. (2021). Nanocrystal quantum dots: from discovery to modern development. *ACS Nano* 15 (4): 6192–6210.

3 Kang, K. and Min, B.I. (1997). Effect of quantum confinement on electron tunneling through a quantum dot. *Physical Review B* 55 (23): 15412–15415.

4 Cordones, A.A. and Leone, S.R. (2013). Mechanisms for charge trapping in single semiconductor nanocrystals probed by fluorescence blinking. *Chemical Society Reviews* 42 (8): 3209–3221.

5 Joughi, Y.D.G. and Sahrai, M. (2022). Spatial-dependent quantum dot-photon entanglement via tunneling effect. *Scientific Reports* 12 (1): 7984.

6 Yeyati, A.L., Cuevas, J.C., López-Dávalos, A., and Martín-Rodero, A. (1997). Resonant tunneling through a small quantum dot coupled to superconducting leads. *Physical Review B* 55 (10): R6137–R6140.

7 Donegá, C.M. (2011). Synthesis and properties of colloidal heteronanocrystals. *Chemical Society Reviews* 40 (3): 1512–1546.

8 García de Arquer, F.P., Talapin, D.V., Klimov, V.I. et al. (2021). Semiconductor quantum dots: technological progress and future challenges. *Science* 373 (6555): eaaz8541.

9 Pu, C., Dai, X., Shu, Y. et al. (2020). Electrochemically-stable ligands bridge the photoluminescence-electroluminescence gap of quantum dots. *Nature Communications* 11 (1): 937.

10 Shirasaki, Y., Supran, G.J., Bawendi, M.G., and Bulović, V. (2012). Emergence of colloidal quantum-dot light-emitting technologies. *Nature Photonics* 7 (1): 13–23.

11 Shen, H., Wang, H., Tang, Z. et al. (2009). High quality synthesis of monodisperse zinc-blende CdSe and CdSe/ZnS nanocrystals with a phosphine-free method. *CrystEngComm* 11 (8): 1733–1738.

12 Lübkemann, F., Rusch, P., Getschmann, S. et al. (2020). Reversible cation exchange on macroscopic CdSe/CdS and CdS nanorod based gel networks. *Nanoscale* 12 (8): 5038–5047.

13 Cho, W., Kim, S., Coropceanu, I. et al. (2018). Direct synthesis of six-monolayer (1.9 nm) thick zinc-blende CdSe nanoplatelets emitting at 585 nm. *Chemistry of Materials* 30 (20): 6957–6960.

14 Wang, F., Chen, B., Pun, E.Y.B., and Lin, H. (2015). Alkaline aluminum phosphate glasses for thermal ion-exchanged optical waveguide. *Optical Materials* 42: 484–490.

15 Wang, F., Chen, B., Pun, E.Y.-B., and Lin, H. (2014). $Dy3^{+}$ doped sodium–magnesium–aluminum–phosphate glasses for greenish–yellow waveguide light sources. *Journal of Non-Crystalline Solids* 391: 17–22.

16 Wang, F., Chen, B.J., Lin, H., and Pun, E.Y.B. (2014). Spectroscopic properties and external quantum yield of $Sm3^{+}$ doped germanotellurite glasses. *Journal of Quantitative Spectroscopy and Radiative Transfer* 147: 63–70.

17 Pu, C., Qin, H., Gao, Y. et al. (2017). Synthetic control of exciton behavior in colloidal quantum dots. *Journal of the American Chemical Society* 139 (9): 3302–3311.

18 Zhang, A., Dong, C., Liu, H., and Ren, J. (2013). Blinking behavior of CdSe/CdS quantum dots controlled by alkylthiols as surface trap modifiers. *The Journal of Physical Chemistry C* 117 (46): 24592–24600.

19 Omogo, B., Aldana, J.F., and Heyes, C.D. (2013). Radiative and nonradiative lifetime engineering of quantum dots in multiple solvents by surface atom stoichiometry and ligands. *The Journal of Physical Chemistry C* 117 (5): 2317–2327.

20 Efros, A.L. and Nesbitt, D.J. (2016). Origin and control of blinking in quantum dots. *Nature Nanotechnology* 11 (8): 661–671.

21 Hohng, S. and Ha, T. (2004). Near-complete suppression of quantum dot blinking in ambient conditions. *Journal of the American Chemical Society* 126 (5): 1324–1325.

22 Rabouw, F.T., Antolinez, F.V., Brechbühler, R., and Norris, D.J. (2019). Microsecond blinking events in the fluorescence of colloidal quantum dots revealed by correlation analysis on preselected photons. *The Journal of Physical Chemistry Letters* 10 (13): 3732–3738.

23 Vaneski, A. (2013). Synthesis and design of hybrid nanaostructures [sic] based on II–VI semiconductor nanocrystals. Doctoral thesis. City University of Hong Kong.

24 Shen, H., Zhou, C., Xu, S. et al. (2011). Phosphine-free synthesis of $Zn_{1-x}Cd_xSe/ZnSe/ZnSe_xS_{1-x}/ZnS$ core/multishell structures with bright and stable blue–green photoluminescence. *Journal of Materials Chemistry* 21 (16): 6046–6053.

25 Cheng, Y., Wan, H., Liang, T. et al. (2021). Continuously graded quantum dots: synthesis, applications in quantum dot light-emitting diodes, and perspectives. *The Journal of Physical Chemistry Letters* 12 (25): 5967–5978.

26 Lim, J., Park, Y.-S., and Klimov, V.I. (2018). Optical gain in colloidal quantum dots achieved with direct-current electrical pumping. *Nature Materials* 17 (1): 42–49.

27 Michler, P. (2003). *Single Quantum Dots: Fundamentals, Applications and New Concepts*. Springer Science & Business Media.

28 Lim, S.Y., Shen, W., and Gao, Z. (2015). Carbon quantum dots and their applications. *Chemical Society Reviews* 44 (1): 362–381.

29 Morozova, S., Alikina, M., Vinogradov, A., and Pagliaro, M. (2020). Silicon quantum dots: synthesis, encapsulation, and application in light-emitting diodes. *Frontiers in Chemistry* 8: 00191.

30 Jang, E., Jun, S., Jang, H. et al. (2010). White-light-emitting diodes with quantum dot color converters for display backlights. *Advanced Materials* 22 (28): 3076–3080.

31 Ziegler, J., Xu, S., Kucur, E. et al. (2008). Silica-coated InP/ZnS nanocrystals as converter material in white LEDs. *Advanced Materials* 20 (21): 4068–4073.

32 Anandan, M. (2008). Progress of LED backlights for LCDs. *Journal of the Society for Information Display* 16 (2): 287–310.

33 Bae, W.K., Park, Y.-S., Lim, J. et al. (2013). Controlling the influence of Auger recombination on the performance of quantum-dot light-emitting diodes. *Nature Communications* 4 (1): 2661.

34 Pietryga, J.M., Park, Y.-S., Lim, J. et al. (2016). Spectroscopic and device aspects of nanocrystal quantum dots. *Chemical Reviews* 116 (18): 10513–10622.

35 Bi, C., Yao, Z., Hu, J. et al. (2023). Suppressing Auger recombination of perovskite quantum dots for efficient pure-blue-light-emitting diodes. *ACS Energy Letters* 8 (1): 731–739.

36 Klimov, V.I. (2014). Multicarrier interactions in semiconductor nanocrystals in relation to the phenomena of Auger recombination and carrier multiplication. *Annual Review of Condensed Matter Physics* 5 (1): 285–316.

37 Klimov, V.I. (2007). Spectral and dynamical properties of multiexcitons in semiconductor nanocrystals. *Annual Review of Physical Chemistry* 58: 635–673.

38 Robel, I., Gresback, R., Kortshagen, U. et al. (2009). Universal size-dependent trend in Auger recombination in direct-gap and indirect-gap semiconductor nanocrystals. *Physical Review Letters* 102 (17): 177404.

39 Chepic, D.I., Efros, A.L., Ekimov, A.I. et al. (1990). Auger ionization of semiconductor quantum drops in a glass matrix. *Journal of Luminescence* 47 (3): 113–127.

40 Tang, J. and Marcus, R.A. (2005). Diffusion-controlled electron transfer processes and power-law statistics of fluorescence intermittency of nanoparticles. *Physical Review Letters* 95 (10): 107401.

41 Frantsuzov, P.A., Volkan-Kacso, S., and Janko, B. (2009). Model of fluorescence intermittency of single colloidal semiconductor quantum dots using multiple recombination centers. *Physical Review Letters* 103 (20): 207402.

42 Shimizu, K.T., Neuhauser, R.G., Leatherdale, C.A. et al. (2001). Blinking statistics in single semiconductor nanocrystal quantum dots. *Physical Review B* 63 (20): 205316.

43 Califano, M. (2011). Off-state quantum yields in the presence of surface trap states in CdSe nanocrystals: the inadequacy of the charging model to explain blinking. *The Journal of Physical Chemistry C* 115 (37): 18051–18054.

44 Rosen, S., Schwartz, O., and Oron, D. (2010). Transient fluorescence of the off state in blinking CdSe/CdS/ZnS semiconductor nanocrystals is not governed by Auger recombination. *Physical Review Letters* 104 (15): 157404.

45 Kagan, C.R., Lifshitz, E., Sargent, E.H., and Talapin, D.V. (2016). Building devices from colloidal quantum dots. *Science* 353 (6302): 5523.

46 Anikeeva, P.O., Madigan, C.F., Halpert, J.E. et al. (2008). Electronic and excitonic processes in light-emitting devices based on organic materials and colloidal quantum dots. *Physical Review B* 78 (8): 085434.

47 Chou, K.F. and Dennis, A.M. (2015). Forster resonance energy transfer between quantum dot donors and quantum dot acceptors. *Sensors (Basel)* 15 (6): 13288–13325.

48 Spanhel, L. and Anderson, M.A. (1990). Synthesis of porous quantum-size cadmium sulfide membranes: photoluminescence phase shift and demodulation measurements. *Journal of the American Chemical Society* 112 (6): 2278–2284.

49 Michalet, X., Pinaud, F.F., Bentolila, L.A. et al. (2005). Quantum dots for live cells, in vivo imaging, and diagnostics. *Science* 307 (5709): 538–544.

50 Lingley, Z., Lu, S., and Madhukar, A. (2011). A high quantum efficiency preserving approach to ligand exchange on lead sulfide quantum dots and interdot resonant energy transfer. *Nano Letters* 11 (7): 2887–2891.

51 Shirasaki, Y., Supran, G.J., Tisdale, W.A., and Bulovic, V. (2013). Origin of efficiency roll-off in colloidal quantum-dot light-emitting diodes. *Physical Review Letters* 110 (21): 217403.

52 Colvin, V.L., Schlamp, M.C., and Alivisatos, A.P. (1994). Light-emitting diodes made from cadmium selenide nanocrystals and a semiconducting polymer. *Nature* 370 (6488): 354–357.

53 Dabbousi, B.O., Bawendi, M.G., Onitsuka, O., and Rubner, M.F. (1995). Electroluminescence from CdSe quantum-dot/polymer composites. *Applied Physics Letters* 66 (11): 1316–1318.

54 Coe, S., Woo, W.-K., Bawendi, M., and Bulović, V. (2002). Electroluminescence from single monolayers of nanocrystals in molecular organic devices. *Nature* 420 (6917): 800–803.

55 Kim, S.H., Man, M.T., Lee, J.W. et al. (2020). Influence of size and shape anisotropy on optical properties of CdSe quantum dots. *Nanomaterials* 10 (8): 1589.

56 Caruge, J.M., Halpert, J.E., Wood, V. et al. (2008). Colloidal quantum-dot light-emitting diodes with metal-oxide charge transport layers. *Nature Photonics* 2 (4): 247–250.

57 Kim, H.Y., Park, Y.J., Kim, J. et al. (2016). Transparent InP quantum dot light-emitting diodes with ZrO_2 electron transport layer and indium zinc oxide top electrode. *Advanced Functional Materials* 26 (20): 3454–3461.

58 Stouwdam, J.W. and Janssen, R.A.J. (2008). Red, green, and blue quantum dot LEDs with solution processable ZnO nanocrystal electron injection layers. *Journal of Materials Chemistry* 18 (16): 1889.

59 Cho, K.-S., Lee, E.K., Joo, W.-J. et al. (2009). High-performance crosslinked colloidal quantum-dot light-emitting diodes. *Nature Photonics* 3 (6): 341–345.

60 Qian, L., Zheng, Y., Xue, J., and Holloway, P.H. (2011). Stable and efficient quantum-dot light-emitting diodes based on solution-processed multilayer structures. *Nature Photonics* 5 (9): 543–548.

61 Dai, X., Zhang, Z., Jin, Y. et al. (2014). Solution-processed, high-performance light-emitting diodes based on quantum dots. *Nature* 515 (7525): 96–99.

62 Yang, Y., Zheng, Y., Cao, W. et al. (2015). High-efficiency light-emitting devices based on quantum dots with tailored nanostructures. *Nature Photonics* 9 (4): 259–266.

63 Manders, J.R., Qian, L., Titov, A. et al. (2015). High efficiency and ultra-wide color gamut quantum dot LEDs for next generation displays. *Journal of the Society for Information Display* 23 (11): 523–528.

64 Wang, L., Lin, J., Hu, Y. et al. (2017). Blue quantum dot light-emitting diodes with high electroluminescent efficiency. *ACS Applied Materials and Interfaces* 9 (44): 38755–38760.

65 Won, Y.-H., Cho, O., Kim, T. et al. (2019). Highly efficient and stable InP/ZnSe/ZnS quantum dot light-emitting diodes. *Nature* 575 (7784): 634–638.

66 Shen, H., Gao, Q., Zhang, Y. et al. (2019). Visible quantum dot light-emitting diodes with simultaneous high brightness and efficiency. *Nature Photonics* 13 (3): 192–197.

67 Vasilopoulou, M., Kim, H.P., Kim, B.S. et al. (2020). Efficient colloidal quantum dot light-emitting diodes operating in the second near-infrared biological window. *Nature Photonics* 14 (1): 50–56.

68 Deng, Y., Peng, F., Lu, Y. et al. (2022). Solution-processed green and blue quantum-dot light-emitting diodes with eliminated charge leakage. *Nature Photonics* 16 (7): 505–511.